Supercontinuum Generation in Inverted Gallium Phosphide-on-Insulator Rib Waveguides

Weiren Cheng[1], Zhaoting Geng[1], Zhuoyu Yu[1], Yihan Liu[1], Yatao Yang[1], Pengzhuo Wu[1], Xiaolun Yu[1], Yifan Wang[1], Changjing Bao[2],Yi Li[1]*, and Qiancheng Zhao[1]*

[1]School of Microelectronics, MOE Engineering Research Center of Integrated Circuits for Next Generation Communications, Southern University of Science and Technology, Shenzhen, Guangdong, China, 518000
[2]Nokia Corporation, New York, NY, USA, 10016

*Corresponding authors: liy37@sustech.edu.cn, zhaoqc@sustech.edu.cn

***Abstract*—We report a GaP-OI integrated photonic platform fabricated by an intermediate layer bonding process. The propagation loss is 23.5 dB/cm for a 1.8 μm-wide waveguide, from which supercontinuum generation was observed.**

Keywords—Nonlinear photonics, gallium phosphide-on-insulator, supercontinuum generation

I. Introduction

The third-order nonlinearity ($\chi^{(3)}$) is one of the most important material properties in integrated nonlinear photonics and is fundamental to a broad range of applications, such as Kerr frequency comb generation [1], supercontinuum generation [2], optical parametric oscillation [3], optical signal processing [4], quantum computing [5], etc. The performance of nonlinear photonic devices rely not only on the material's nonlinear response but also on the local optical intensity. Thus, it is preferable to use materials with large $\chi^{(3)}$ nonlinear coefficients and large linear refractive indices. The silicon-on-insulator (SOI) platform seems to be a suitable solution, but rather struggles with two-photon absorption (TPA) loss at telecom wavelengths, which limits its nonlinear applications mainly in the mid-infrared spectra [6]. Therefore, finding alternative materials that have low TPA loss at telecom bands and high $\chi^{(3)}$ nonlinearity is of utmost interest to the integrated nonlinear photonics community.

Gallium phosphide (GaP) is a promising material thanks to its excellent linear and nonlinear optical properties [7]. First, GaP has negligible two-photon absorption (TPA) at wavelengths above 1.1 μm, enabling high-power operation in all telecom bands. Second, GaP has large $\chi^{(3)}$ coefficients that is nearly 2 orders of magnitude larger than Si_3N_4 and $LiNbO_3$. Third, the refractive index of GaP is high (~3.05 in C-band [8]), rendering tight mode confinement in nanostructures possible [9]. Besides, GaP has a wide transparent window from 550 nm to 11 μm. In addition, its non-central symmetric crystal structure enables intrinsic large $\chi^{(2)}$ nonlinearity, which facilitates frequency conversion from telecom to visible wavelengths.

In order to fully release the material's potential, GaP-on-insulator (GaP-OI) architecture was proposed by using the direct bonding process [10], and has achieved rapid progress in recent years [11]. However, the direct bonding method usually requires surface treatment to form ultrasmooth interfaces, which increases the fabrication complexity and cost. An alternative is to use intermediate layer bonding process, which can relax the smoothness requirement and is more tolerable to the lattice mismatch and thermal mismatch. In this work, we report a low-cost GaP-OI heterogeneous integration method based on the intermediate layer bonding process. The "etch-n-transfer" fabrication flow and the shallow dry etching process render wafer-scale fabrication possible, and produce the inverted rib waveguide structures. The fabricated 1.8 μm-wide GaP-OI waveguide has a propagation loss of 23.5 dB/cm. Supercontinuum generation (SCG) was observed on the all-normal dispersion GaP-OI waveguides based on the self-phase modulation (SPM) effect. To the best of the authors' knowledge, it is the first time to report SCG on the GaP-OI waveguides. The nonlinear refractive index of GaP is extracted to be $n_2 = 1.9 \times 10^{-17}$ m^2W^{-1}. Combined with the characterized linear and nonlinear properties, the GaP-OI platform shows great potential in large-scale manufacturing on-chip nonlinear photonic devices such as frequency comb microresonators [12], [13].

II. Fabrication

The fabrication process of the inverted GaP-OI waveguide devices is shown in Fig. 1. The 600 nm-thick GaP epitaxial film is grown on a 200 nm-thick AlGaInP buffer layer, which is used to reduce the lattice mismatch between the GaP epi layer and the GaAs substrate. A ~1120 nm thick photoresist is spun on top of the GaP epi wafer and is exposed by an i-line UV lithography machine with an intensity of 8.0 mW/cm^2 and an exposure time of 4 s. The photoresist (PR) is developed in a KOH-based developer followed by hard baking.

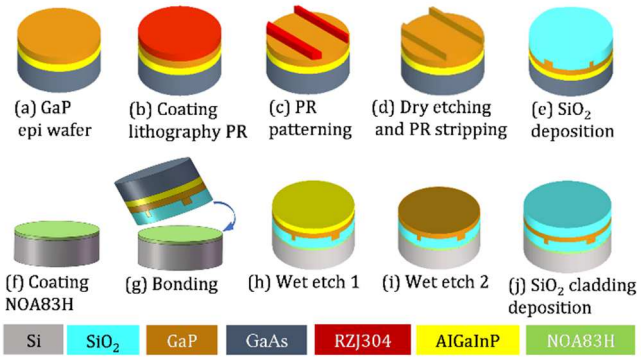

Fig. 1 Fabrication flow of the inverted GaP-OI rib waveguides.

The GaP epi layer is then etched by a chlorine-based formulation using an inductively coupled plasma etching machine [8], followed by photoresist stripping. Shown in. Fig. 2(a) is a GaP rib waveguide after photoresist removal. A 2 μm-thick SiO_2 layer is coated on the GaP surface using a plasma enhanced chemical vapor deposition (PECVD) machine. After forming the GaP/SiO_2 interface, the patterned GaP epi wafer is bonded to a Si substrate via an optical adhesive layer (NOA83H). Once the wafers are firmly bonded, wet etching can be carried out to remove the host materials GaAs [14]. A dip in the buffered oxide etcher solution washes the AlGaInP sacrificial layer away, followed by deionized (DI) water rinsing to complete the wet etching process. Finally, the backside of the GaP slab is coated with a layer of 2 μm thick PECVD SiO_2 for surface protection and passivation. Shown in Fig. 2(b) is the SEM image of the cross section of inverted GaP-OI rib

waveguide. The fabricated GaP-OI waveguides have a rib height of 167.5 nm. Their core thickness is measured to be 577 nm, thinner than the GaP film thickness in the epi wafer. The discrepancy may be caused by the combined effects of film thickness variation in the growth step and over-etching GaP in the wet etching step.

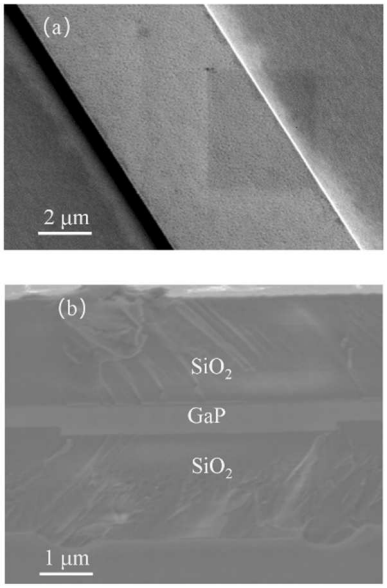

Fig. 2 (a) The SEM image of a GaP rib waveguide after stripping photoresist. (b) is the SEM image of the cross section of inverted GaP-OI rib waveguide.

III. Propagation Loss Characterization

The impact of rib height and waveguide width on the waveguide effective mode index (n_{eff}) is illustrated in Fig. 3(a). Below the width of 1 μm, our waveguide operates in the single mode condition. The waveguide propagation loss at 1550 nm wavelength is measured by the cut-back method. The propagation loss of the fundamental TE mode on a 1.8 μm-wide waveguide is extracted to be 23.5 dB/cm based on the linear fitting. The intercept on the *y*-axis indicates that the coupling loss is 15.9 dB/facet, as shown in Fig. 3(b). Our waveguide propagation loss is on par with the reported values [10], [14].

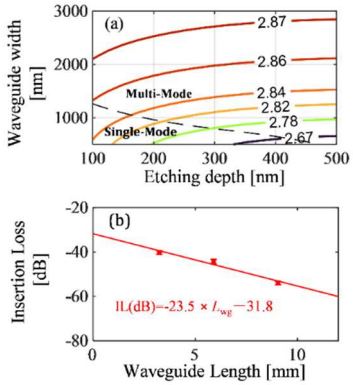

Fig. 3 (a) The effective refractive index (n_{eff}) of the fundamental mode as a function of the etch depth and the waveguide width. The dashed line divides the single-mode and multi-mode regions. (b) The waveguide propagation loss (slope) is 23.5 dB/cm for a 1.8 μm wide GaP-OI waveguide.

IV. Supercontinuum Generation

We did SCG experiment based on the self-phase modulation (SPM) effect from high energy pulses to study the nonlinear properties of the GaP-OI waveguide. The schematic of the experimental setup for supercontinuum generation in the GaP-OI waveguides is shown in Fig. 4. A mode-locked femtosecond laser (FL) provides pulses with 500 fs duration at a repetition rate of 80 MHz centered at 1564 nm. Attenuators were connected to the laser output to adjust the pulse energy. The pulses were adjusted to be in quasi-TE polarization through a fiber polarization controller (PFC) and fed into the GaP-OI waveguides using a lensed fiber (LF). The output light was collected by another lensed fiber and sent to an optical spectrum analyzer (OSA).

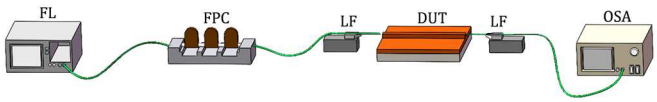

Fig. 4 The schematic of the spectrum broadening experiment setup. FL: femtosecond laser, FPC: fiber polarization controller, LF: lensed fiber, DUT: device under test, OSA: optical spectrum analyzer.

The solid lines in Fig. 5 show the measured output spectra from a 1.8 μm wide GaP-OI waveguide at different power levels. The variation of the on-chip power leads to different stages of SPM. Since the waveguide has a normal dispersion, the spectral profile exhibits a characteristic mesa shape with split peaks, which is used to estimate the maximum nonlinear phase shift. We extracted the 1.8 μm wide waveguide's nonlinear parameter to be 90.9 $\text{m}^{-1}\text{W}^{-1}$, and calculated the nonlinear refractive index of GaP to be 1.9×10^{-17} m^2W^{-1}. The TPA of the GaP is assumed to be negligible and not included in our calculation. The measured n_2 is in a reasonable agreement with the reported values in literature that are in the order of 10^{-17} m^2W^{-1} [11].

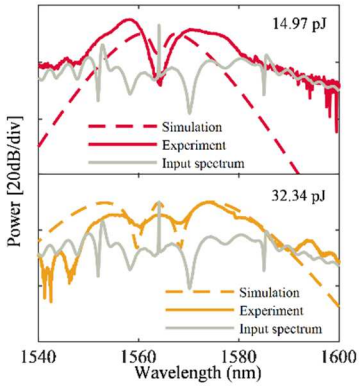

Fig. 5 Measured and simulated output spectra at different pulse energies from the waveguide with a width of 1.8 μm.

Using the extracted n_2 value and propagation loss, we simulated the SCG output spectra by solving the Generalized Nonlinear Schrödinger Equation (GNLSE) [15]:

$$\frac{\partial A}{\partial z}+\frac{\alpha}{2}A-i\sum_{k\geq 2}\beta_{\text{k}}\frac{i^k}{k!}\frac{\partial^k A}{\partial T^k}=i\gamma\left(1+i\tau_{\text{s}}\frac{\partial}{\partial T}\right)\left[(1-f_{\text{r}})|A|^2A+f_{\text{r}}A\int_0^{\infty}h_{\text{r}}(T')|A(z,T-T')|^2dT'\right] \quad (1)$$

where A is the pulse envelope, β_{k} is the dispersion coefficients, and τ_{s} is the characteristic time scale of self-steepening. The integral term describes Raman effect: f_{r} is the Raman contribution and $h_{\text{r}}(T)$ is the Raman temporal response. The simulated spectra are shown as the dashed lines in Fig. 5. Good similarity between the measured results and simulation is obtained, which verifies the reasonability of the extracted n_2.

In summary, we report an integrated GaP-OI platform using an "etch-n-transfer" intermediate layer bonding process. The fabricated waveguides have propagation loss of 23.5 dB/cm. SCG is demonstrated for the first time in the all-normal dispersion GaP-OI waveguides based on SPM effect, further expanding the capabilities

of GaP-OI integrated photonics. The prominent third order nonlinearity, tight mode confinement, and moderate propagation loss enable the development of novel GaP-OI devices with unprecedented performance in nonlinear applications.

V. Acknowledgment

This work was partially supported by Basic and Applied Basic Research Foundation of Guangdong Province (2021B1515120074, 2023A1515012141), National Natural Science Foundation of China (62205137), Wuhan National Laboratory for Optoelectronics (2021WNLOKF001). The authors acknowledge the assistance of SUSTech Core Research Facilities.

VI. References

[1] A. L. Gaeta, M. Lipson, and T. J. Kippenberg, "Photonic-chip-based frequency combs," *Nature Photonics*, vol. 13, no. 3, Art. no. 3, Mar. 2019, doi: 10.1038/s41566-019-0358-x.

[2] S. May, M. Clerici, and M. Sorel, "Supercontinuum generation in dispersion engineered AlGaAs-on-insulator waveguides," *Sci Rep*, vol. 11, no. 1, Art. no. 1, Jan. 2021, doi: 10.1038/s41598-021-81555-3.

[3] X. Ji *et al.*, "Ultra-low-loss on-chip resonators with sub-milliwatt parametric oscillation threshold," *Optica, OPTICA*, vol. 4, no. 6, pp. 619–624, Jun. 2017, doi: 10.1364/OPTICA.4.000619.

[4] M. Pu *et al.*, "Ultra-Efficient and Broadband Nonlinear AlGaAs-on-Insulator Chip for Low-Power Optical Signal Processing," *Laser & Photonics Reviews*, vol. 12, no. 12, p. 1800111, 2018, doi: 10.1002/lpor.201800111.

[5] X. Lu *et al.*, "Chip-integrated visible–telecom entangled photon pair source for quantum communication," *Nat. Phys.*, vol. 15, no. 4, pp. 373–381, Apr. 2019, doi: 10.1038/s41567-018-0394-3.

[6] A. G. Griffith *et al.*, "Silicon-chip mid-infrared frequency comb generation," *Nat Commun*, vol. 6, no. 1, p. 6299, Feb. 2015, doi: 10.1038/ncomms7299.

[7] W. Xie *et al.*, "Nonlinear response of a gallium phosphide nanopatterned photonic waveguide in the CW regime," *Opt. Lett.*, vol. 44, no. 11, p. 2823, Jun. 2019, doi: 10.1364/OL.44.002823.

[8] J. Cambiasso, G. Grinblat, Y. Li, A. Rakovich, E. Cortés, and S. A. Maier, "Bridging the Gap between Dielectric Nanophotonics and the Visible Regime with Effectively Lossless Gallium Phosphide Antennas," *Nano Lett.*, vol. 17, no. 2, pp. 1219–1225, Feb. 2017, doi: 10.1021/acs.nanolett.6b05026.

[9] Y. Yan, T. Zhu, Q. Zhao, R. Berté, and Y. Li, "Launching directional hypersonic surface waves in monolithic gallium phosphide nanodisks: two holes are better than one," *Nanoscale*, vol. 15, no. 7, pp. 3318–3325, Jan. 2023, doi: 10.1039/D2NR05729H.

[10] K. Schneider, P. Welter, Y. Baumgartner, H. Hahn, L. Czornomaz, and P. Seidler, "Gallium Phosphide-on-Silicon Dioxide Photonic Devices," *J. Lightwave Technol., JLT*, vol. 36, no. 14, pp. 2994–3002, Jul. 2018.

[11] D. J. Wilson *et al.*, "Integrated gallium phosphide nonlinear photonics," *Nat. Photonics*, vol. 14, no. 1, pp. 57–62, Jan. 2020, doi: 10.1038/s41566-019-0537-9.

[12] Z. Geng *et al.*, "Dispersion-flattened concentric structure for microcomb bandwidth broadening in GaP-OI resonators," *J. Opt. Soc. Am. B, JOSAB*, vol. 40, no. 3, pp. 673–681, Mar. 2023, doi: 10.1364/JOSAB.477493.

[13] H. Ji *et al.*, "Design of Partially Etched GaP-OI Microresonators for Two-Color Kerr Soliton Generation at NIR and MIR," in *2022 Asia Communications and Photonics Conference (ACP)*, Nov. 2022, pp. 1622–1625. doi: 10.1109/ACP55869.2022.10089110.

[14] A. P. Anthur *et al.*, "Second harmonic generation in gallium phosphide nano-waveguides," *Opt. Express, OE*, vol. 29, no. 7, pp. 10307–10320, Mar. 2021, doi: 10.1364/OE.409758.

[15] J. M. Dudley and J. R. Taylor, Eds., *Supercontinuum generation in optical fibers*. Cambridge ; New York: Cambridge University Press, 2010.